Journal of Naval Architecture and Marine Engineering
December, 2023
https://dx.doi.org/10.3329/jname.v20i2.67298 *http://www.banglajol.info*

HEAT TRANSFER WITH VISCOUS DISSIPATION AND ENTROPY GENERATION IN A NANOFLUID FLOW THROUGH A POROUS MEDIUM

B. K. Swain[1*], S. Sahu[2], K. L. Ojha[3], G. C. Dash[4]
[1]Department of Mathematics, Agarpara College, Agarpara, Bhadrak, Odisha, India, bharatkeshari1@gmail.com
[2]Department of Mathematics, IGIT, Sarang, Odisha, India, sipunsahu534@gmail.com
[3]Department of Mathematics, S.O.A, Deemed to be University, Bhubaneswar, India, kanakalataojha@soa.ac.in
[4]Department of Mathematics, S.O.A, Deemed to be University, Bhubaneswar, India, gcdash45@gmail.com

Abstract:

This article describes the Al_2O_3/Cu/Ag-H_2O nanofluid stagnation-point flow through a porous medium with emphasis on heat transfer as well as magnetohydrodynamic (MHD) behavior and entropy generation. The main motivation is to do the MHD flow of nanofluid and look into the repercussions of viscous dissipation, which has many applications in various industries, especially the extrusion process where the durability of the end product is of interest. The governing equations are solved using similarity transformations and DTM-Padé approximations, and the solutions are then compared to the outcomes of the numerical technique (shooting technique and Runge-Kutta 4th order method), which validates the accuracy of the research. The ranges of the parameters are taken as $-2< Q < 3$, $0 < G_r < 6$, $0 < G_c < 6$, $0 < Br < 3$, $0< \phi < 0.3$. Some important findings are: entropy generation is to decrease for higher values of Br in a streamline manner within asymptotic pattern; viscous heating is dominant in the neighborhood of the plate for higher value of Br and for small values the distribution is smooth across the flow field; decrease in entropy generation for higher value of Br shows that there is a base value or residue left over energy in the process of entropy generation, which is important in its own revelation and application basis.

Keywords: MHD, viscous dissipation, heat source/sink, nanofluid, porous medium, entropy generation.

NOMENCLATURE

a	Constant number	G_r	Thermal Grashof number
B	applied magnetic field	G_c	Mass Grashof number
Br	Brinkman number	Ha	Hartman number
C	Nanoparticles concentration	k	thermal conductivity
C_f	coefficient of skin friction	K_p	Permeability parameter
C_p	Specific heat	L	Reference length
C_∞	Free stream concentration	M	Magnetic parameter
D	mass diffusivity	Nu_x	Nusselt number
Da	Dracy number	P	fluid pressure
E_c	Eckert number	P_r	Prandtl number
q_r	flux of radiant heat	***Greek symbols***	
Q	Heat source parameter	Ω	dimensionless temperature
R	Radiation parameter	σ_s	electrical conductivity of base fluid
R_c	Chemical reaction parameter	σ_f	electrical conductivity of nanofluid
S	Suction/blowing parameter	ϕ	Solid volume fraction
S_c	Schmidt number	ν_f	kinematic viscosity
Sh_x	Sherwood number	ρ	density
T	fluid temperature	q_w	heat flux

1813-8535 (Print), 2070-8998 (Online) Received on: June, 2023

U	free stream velocity	τ_w	skin friction
u , v	velocity components	p_m	mass flux

1. Introduction

Choi (2009) mentioned a new category of fluid known as nanofluid. This fluid is composed of conventional base fluids such as oil, water, ethylene glycol, and nanoparticles such as graphite, carbon nanotubes (CNTs), silver, copper, copper oxide, and alumina (Ladjevardi et al., 2013, Aravind et al., 2011), ceramics and carbide, (Sadeghinezhad et al., 2016), Ijam et al., 2015)). Since nanoparticles possess improved thermal properties, many studies have been conducted on their functions in heat pumps, air conditioning and other thermal equipment in order to increase the reliability and efficacy of the systems (Khanafer and Vafai, 2001, Ali et al., 2003, Shafahi et al., 2010). Using different kinds and shapes of nanoparticles, Haque et al. (2016) clarified the properties of a home refrigerator. They found that their system consumed 27.73% and 14.19% less energy when Al_2O_3 and TiO_2 nanoparticles were added to polyolester (POE) oil, respectively, at 0.1% volume fractions. According to Bi et al. (2008), the R134a refrigerator was found to be lubricated using mineral oil rather than polyolester oil and TiO_2 nanoparticles. Bagh et al. (2022) investigated the MHD hybrid nanofluid flow over an inclined surface using finite element simulation describing the significance of gravity modulation and heat source/sink. They found that the fluctuation of skin-friction and heat flux gradient improves with larger inputs of amplitude of modulation. Biswal et al. (2022) numerically investigates nanofluid flow between two inclined stretchable walls and observed that in both divergent and convergent cases velocity increases and temperature decreases with the increasing values of stretching/shrinking parameter.

Some studies investigate the flow at the nanofluid stagnation point to develop thermal properties. In order to better understand stagnation point nanofluid flow across a stretched surface, Mustafa et al. (2011) and Bachok et al. (2013) took Brownian motion and thermophoresis into account. Kameswaran et al. (2013) assert that dual solutions are present for some values of the stretching/shrinking parameter. Additionally, they describe how homogeneous and heterogeneous reactions affect stagnation point flow. The MHD stagnation point nanofluid flow on a stretching/shrinking surface was also clarified by Mansur et al. (2015), who described the uniqueness of solution in stretching case. Mohamed et al. (2015) and Mahatha (2015) explored the slip condition at the nano and micro-scales, where it is found to be more realistic, in order to better understand how velocity slip influences nanofluid stagnation point flow.

Geophysical fluxes, high viscosity flows like oil and polymers, aerodynamic heating, etc. all depend heavily on free convective and viscous dissipative flow (Swain et al., 2020). The Eckert number, which is used to describe the viscous dissipation in general, is interpreted as the kinetic energy to heat transition enthalpy driving force ratio (Jusoh, 2019). Numerous researches have examined how viscous dissipation affects fluid motion. The generation of extra heat and a poor heat transfer rate in the boundary layer region, according to Kameswaran et al. (2012), are both influenced by the magnetic field and viscous dissipation factors. Larger viscous dissipation-related Eckert numbers are associated with higher temperatures while lower Nusselt numbers, according to Sheikholeslami et al. (2014). According to Mabood et al. (2015), the properties of viscous stress, which result in a slower rate of heat transfer and a faster rate of mass transfer, cause the transformation of kinetic energy into internal energy to provide heat source. Syuhada et al. (2019) described the stability of the MHD stagnation point flow with a focus on the viscous dissipation. Numerous investigations have been conducted to determine how viscous dissipation affects the flows of nanofluids (Ali et al. (2019), Ali et al.(2021), Hussain (2017), Parida et al. (2021)). Situations involving dissociating fluids and moving fluids that involve chemical processes can be used to illustrate the relevance of heat generation. It is possible that variations in temperature distribution, specifically as a result of the impact of heat generation, will affect particle accumulation rates in electronic devices, nuclear reactors etc. Many additional studies have focused on how various flow forms are affected by interactions between chemical reaction and heat sources/sinks (Biswal et al.(2022), Swain (2021), Swain et al. (2021)).

Entropy is the measure of thermal energy per unit temperature that is unavailable for doing useful work in a thermodynamic system. It is also a measure of the molecular disorder or randomness of the system. Physically, entropy production, which is widely observed in all types of designs, is characterised by irreversibility in a thermodynamical system. The generation of entropy has a significant impact on the efficiency of thermal system. Increased generation rates degrade productive work and reduce system effectiveness. Bejan (1982) and Bejan (1996) introduced the Entropy Generation Minimization (EGM) method to reduce the amount of disorder that results from a process, notably in the heat transfer areas. Numerous writers have examined the entropy production

in MHD flow of nanofluids in different geometries (Sohel (2013), Moghaddami (2012), Shahi (2011)) and attempted to reduce the disorderness for the improved performance of system.

The present study has many engineering applications such as in crude oil extraction, heat exchanger, refrigerator, cancer therapy, cooling systems of most of the processing plants, vehicles air conditioning system in transportation etc.

The objective of the current research is to look at how a nanofluid with an MHD stagnation point (Al_2O_3/Cu/Ag-H_2O) flows over a flat plate and transfers heat while being affected by viscous dissipation and a heat source due to the numerous applications stated above. The novelties of this study include:

(i) To solve the governing equations numerically and validate the solution so obtained with the semi analytical method i.e. DTM-Padé approximation.
(ii) To analyze the impacts of heat source/sink and viscous dissipation.
(iii) To examine how entropy is produced in thermal systems.

2. Formulation of the problem

In Fig. 1, a MHD nanofluid flow with uniform suction/blowing is depicted across a flat plate. The incompressible electrically conducting and chemically reactive nanofluid flow is subjected to a transverse magnetic field in the current analysis with a weak magnetic induction $\vec{B}$ (0, B_0, 0), and as a result, the magnetic Reynolds number is so low that the induced magnetic field can be disregarded. The fluid flow in a porous material is investigated using Darcy's law. T_w and T_∞ , respectively, are the surface and ambient temperatures. *U*, the free stream velocity and T_0, the temperature increase rate.

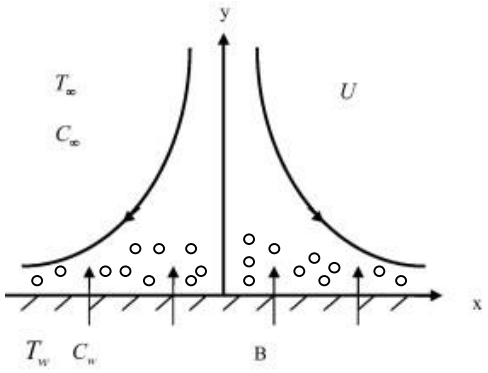

Figure1: Physical flow of the problem

The governing equations listed below are conferred as (cf. Zhang et al. (2014)),

$$\frac{\partial u}{\partial x}+\frac{\partial v}{\partial y}=0, \tag{1}$$

$$u\frac{\partial u}{\partial x}+v\frac{\partial u}{\partial y}=-\frac{1}{\rho_{nf}}\frac{\partial p}{\partial x}+\frac{\mu_{nf}}{\rho_{nf}}\frac{\partial^2 u}{\partial y^2}-\frac{\mu_{nf}}{\rho_{nf}K_p^{*}}u-\frac{\sigma_{nf}B^2}{\rho_{nf}}u+g\beta(T-T_\infty)+g\beta_c(C-C_\infty), \tag{2}$$

$$u\frac{\partial T}{\partial x}+v\frac{\partial T}{\partial y}=\alpha_{nf}\frac{\partial^2 T}{\partial y^2}-\frac{1}{(\rho c_p)_{nf}}\frac{\partial q_r}{\partial y}+\frac{\mu_{nf}}{(\rho c_p)_{nf}}\left(\frac{\partial u}{\partial y}\right)^2+\frac{Q^{*}(T-T_\infty)}{(\rho c_p)_{nf}}, \tag{3}$$

$$u\frac{\partial C}{\partial x}+v\frac{\partial C}{\partial y}=D\frac{\partial^2 C}{\partial y^2}-R_c^{*}(C-C_\infty), \tag{4}$$

with the conditions

$$u=0, v=v_w, T=T_w=T_\infty+T_0\exp\left(\frac{x}{2L}\right), C=C_w=C_\infty+C_0\exp\left(\frac{x}{2L}\right) \text{ at } y=0, \tag{5}$$

$$u \to U = a\exp\left(\frac{x}{L}\right), T \to T_\infty, C \to C_\infty \text{ as } y \to \infty, \tag{6}$$

where $R_c^*(x) = R_{c0}\exp(x/L)$, variable chemical reaction, R_{c0}, a constant. $v_w(x) = v_0\exp(x/2l)$, the suction/blowing velocity. Physically, $v_w(x) < 0$ means injection and $v_w(x) > 0$ implies suction. α_{nf}, the thermal diffusivity of nanofluid, μ_{nf}, the nanofluid viscosity, ρ_{nf}, the nanofluid density and satisfying

$$\alpha_{nf} = \frac{k_{nf}}{(\rho C_p)_{nf}}, \rho_{nf} = (1-\phi)\rho_f + \phi\rho_s, \mu_{nf} = \frac{\mu_f}{(1-\phi)^{2.5}}$$
$$\frac{k_{nf}}{k_f} = \frac{(k_s+2k_f)-2\phi(k_f-k_s)}{(k_s+2k_f)+\phi(k_f-k_s)}, (\rho C_p)_{nf} = (1-\phi)(\rho C_p)_f + \phi(\rho C_p)_s, \sigma_{nf} = (1-\phi)\sigma_f + \phi\sigma_s \tag{7}$$

Table.1: Thermo physical properties

Physical properties	Fluid phase (water)	Cu	Al_2O_3	Ag
$C_p(J/kgK)$	4179	385	765	235
$\rho(kg/m^3)$	997.1	8933	3970	10.50
$k(W/mK)$	0.613	400	40	429
$\sigma(S/m)$	$5.5\text{x}10^{-6}$	$59.6\text{x}10^{6}$	$35\text{x}10^{6}$	$63.01\text{x}10^{6}$

Equation (2) reduces to

$$U\frac{dU}{dx} = -\frac{1}{\rho_{nf}}\frac{\partial p}{\partial x} - \frac{\mu_{nf}}{\rho_{nf}K_p}U - \frac{\sigma_{nf}B^2}{\rho_{nf}}U \tag{8}$$

in free-stream.

From equations (2) & (8) , we getx

$$u\frac{\partial u}{\partial x} + v\frac{\partial u}{\partial y} = U\frac{dU}{dx} + \frac{\mu_{nf}}{\rho_{nf}}\frac{\partial^2 u}{\partial y^2} - \left(\frac{\mu_{nf}}{\rho_{nf}K_p^*} + \frac{\sigma_{nf}B^2}{\rho_{nf}}\right)(u-U) + g\beta(T-T_\infty) + g\beta_c(C-C_\infty), \tag{9}$$

where $K_p = K_{p0}\exp(-x/L)$, K_{p0}, the initial permeability, $B = B_0\exp(x/2L)$,

$q_r = -4\sigma_1\partial T^4/3k_1\partial y$, where σ_1 and k_1 are the constant of Stefan-Boltzmann and coefficient of absorption, respectively according to approximation of Rosseland. Utilizing Taylor's series T^4 is expanded about T_∞ as $T^4 \cong 4T_\infty{}^3T - 3T_\infty{}^4$ ignoring the terms of higher order and then we get

$$\frac{\partial q_r}{\partial y} = -\frac{16}{3}\frac{\sigma_1}{k_1}T_\infty{}^3\frac{\partial^2 T}{\partial y^2} \quad . \tag{10}$$

Now from equation (3), we have

$$u\frac{\partial T}{\partial x} + v\frac{\partial T}{\partial y} = \alpha_{nf}\frac{\partial^2 T}{\partial y^2} + \frac{1}{(\rho c_p)_{nf}}\frac{16\sigma_1 T_\infty{}^3}{3k_1}\frac{\partial^2 T}{\partial y^2} + \frac{\mu_{nf}}{(\rho c_p)_{nf}}\left(\frac{\partial u}{\partial y}\right)^2 + \frac{Q^*(T-T_\infty)}{(\rho c_p)_{nf}}. \tag{11}$$

Introducing the stream function ψ ,

$$u = \frac{\partial\psi}{\partial y}, v = -\frac{\partial\psi}{\partial x}. \tag{12}$$

and utilizing the non-dimensional quantities

$$\eta = y\sqrt{\frac{a}{2\nu_f L}}\exp\left(\frac{x}{2L}\right), \psi = \sqrt{2aL\nu_f}\, f(\eta)\exp\left(\frac{x}{2L}\right),\ \theta(\eta) = \frac{T-T_\infty}{T_w-T_\infty},\ \gamma(\eta) = \frac{C-C_\infty}{C_w-C_\infty}, \quad (13)$$

in equations (9), (11) and (4), we get

$$\frac{1}{\phi_1} f''' + ff'' + 2(1-f'^2) + \left(\frac{1}{\phi_1}K_p + \frac{\phi_4}{\phi_2}M\right)(1-f') + G_r\theta + G_c\gamma = 0, \quad (14)$$

$$\left[\frac{k_{nf}}{\phi_3 k_f} + \frac{R}{\phi_3 k_f}\right]\theta'' + P_r\left(f\theta' - f'\theta + E_c\frac{1}{\phi_3(1-\phi)^{2.5}}f'' + \frac{1}{\phi_3}Q\theta\right) = 0, \quad (15)$$

$$\gamma'' + S_c(f\gamma' - f'\gamma - R_c\gamma) = 0. \quad (16)$$

The reduced boundary conditions are:

$$f = S,\ f' = 0, \theta = 1, \gamma = 1 \text{ at } \eta = 0 \quad (17)$$

$$f' = 1, \theta = 0, \gamma = 0 \text{ as } \eta \to \infty \quad . \quad (18)$$

The associated parameters are

$$K_p = \frac{2L\nu_f}{ak_0}, M = \frac{2\sigma_f B_0{}^2 L}{a\rho_f}, R = \frac{16\sigma_1 T_\infty{}^3}{3k}, S = \frac{\nu_0}{\sqrt{a\nu_f/2L}}, S_c = \frac{\nu_f}{D}, R_c = \frac{2LK_0}{a}, P_r = \frac{\nu_f}{\alpha_f},$$

$$G_r = \frac{2Lg\beta(T_w-T_\infty)}{U^2}, G_c = \frac{2Lg\beta_c(C_w-C_\infty)}{U^2}, E_c = \frac{U^2}{(T_w-T_\infty)(C_p)_f}, Q = \frac{2LQ^*}{U(\rho C_p)_f}, B_r = E_c P_r \quad (19)$$

$$\phi_1 = (1-\phi)^{2.5}[(1-\phi) + \phi\rho_s/\rho_f],$$

$$\phi_2 = (1-\phi) + \phi\rho_s/\rho_f,$$

$$\phi_3 = (1-\phi) + \phi(\rho C_p)_s/(\rho C_p)_f,$$

$$\phi_4 = (1-\phi) + \phi\sigma_s/\sigma_f,$$

The quantities like coefficient of skin friction, Nusselt and Sherwood number are of physical interests which are respectively

$$C_f = \frac{\tau_w}{\rho_f U^2}, Nu_x = \frac{xq_w}{k_f(T_w-T_\infty)}, Sh_x = \frac{xp_m}{D(C_w-C_\infty)} \quad (20)$$

where

$$\tau_w = \mu_{nf}\left(\frac{\partial u}{\partial y}\right)_{y=0}, q_w = -k_{nf}\left(\frac{\partial T}{\partial y}\right)_{y=0}, p_w = -D\left(\frac{\partial C}{\partial y}\right)_{y=0}. \quad (21)$$

Putting (21) into (20), we get

$$(2L/x)(1-\phi)^{2.5} C_f\, \mathrm{Re}_x{}^{1/2} = f''(0), Nu_x\, \mathrm{Re}_x{}^{-1/2}(k_f/k_{nf}) = -\theta'(0), Sh_x\, \mathrm{Re}_x{}^{-1/2} = -\gamma'(0). \quad (22)$$

where Re_x, the local Reynolds number defined by $\mathrm{Re}_x = Ux^2/(2L\nu_f)$.

3. Entropy Generation analysis:

Following is the entropy formation rate when a magnetic field and a medium's permeability are present.

$$E_G = \frac{k}{T_\infty{}^2}\left(\frac{\partial T}{\partial y}\right)^2 + \frac{D}{C_\infty}\left(\frac{\partial C}{\partial y}\right)^2 + \frac{D}{T_\infty}\frac{\partial T}{\partial y}\frac{\partial C}{\partial y} + \frac{\mu}{T_\infty}\left(\frac{\partial u}{\partial y}\right)^2 + \frac{\sigma B_0{}^2 u^2}{T_\infty} + \frac{\mu}{T_\infty K_p}u^2 \quad (23)$$

The final three terms correspond to the entropy produced by joule heating, Darcy dissipation, and viscous dissipation, respectively.

The number representing the entropy generation is $Ns = \frac{E_G}{E_{G0}}$, (24)

where $E_{G0} = \frac{k(\Delta T)^2}{x^2 T_\infty{}^2}$, the rate of characteristic entropy produced. (25)

From equations (13), (28), (29) and (30),

$$Ns = \mathrm{Re}_x\,\theta'^2 + \alpha_1\,\mathrm{Re}_x\,\gamma'^2 + \alpha_2\,\mathrm{Re}_x\,\theta'\gamma' + \frac{Br\,\mathrm{Re}_x}{\Omega}\,f''^2 + \frac{Ha^2 Br}{\Omega}\,f'^2 + \frac{Br}{Da\Omega}\,f'^2, \tag{26}$$

where

$$\mathrm{Re}_x = \frac{U_w x}{\nu}, Br = \frac{\mu U_w{}^2}{k\Delta T}, \frac{1}{Da} = \frac{x^2}{K_p}, \Omega = \frac{\Delta T}{T_\infty}, Ha = B_0 x\sqrt{\frac{\sigma}{\mu}}, \alpha_1 = \frac{DT_\infty{}^2}{kC_\infty}\left(\frac{\Delta C}{\Delta T}\right)^2, \alpha_2 = \frac{DT_\infty}{k}\left(\frac{\Delta C}{\Delta T}\right)$$

4. Method of Solution:

(a) DTM solution

The differential transformation of $w(t)$ is expressed as

$$W(k) = \frac{1}{k!}\left[\frac{d^k w(t)}{dt^k}\right]_{t=t_0}, k = 0,1,2,3....., \tag{27}$$

where $w(t)$is the inverse transformation ofW (k) i.e

$$w(t) = \sum_{k=0}^{\infty} W(k)(t-t_0)^k \approx \sum_{k=0}^{n} W(k)(t-t_0)^k \tag{28}$$

From the definitions (27) and (28), some properties are given in Table 2.

We are required to solve equations (14)- (16)subject to the conditions

$$f(0) = S,\ f'(0) = 0,\ f''(0) = 2\alpha_1 \tag{29}$$

$$\theta(0) = 1, \theta'(0) = \alpha_2 \tag{30}$$

$$\gamma(0) = 1, \gamma'(0) = \alpha_3\,. \tag{31}$$

Taking transformations of equations (29)-(31), we get

$$F(0) = S, F(1) = 0, F(2) = \alpha_1 \tag{32}$$

$$G(0) = 1, G(1) = \alpha_2 \quad , \tag{33}$$

$$H(0) = 1, H(1) = \alpha_3 \quad , \tag{34}$$

the unknowns α_1, α_2 and α_3 are calculated.

Table 2: Fundamental operations

Sl.No.	Original function	Transformed function
1	$w(t) = c_1 w_1(t) + c_2 w_2(t)$	$W(k) = c_1 W_1(k) + c_2 W_2(k)$
2	$w(t) = \frac{d^n w_1(t)}{dt^n}$	$W(k) = (k+1)(k+2)...(k+n)W_1(k+n)$
3	$w(t) = w_1(t) w_2(t)$	$W(k) = \sum_{i=0}^{k} W_1(i) W_2(k-i)$
4	$w(t) = t^m$	$W(k) = \delta(k-m)$

Transforming of Equations. (14)-(16), we have

$$\frac{1}{\phi_1}(k+1)(k+2)(k+3)F(k+3)$$
$$+\sum_{i=0}^{k}\left[(k-i+1)(k-i+2)F(i)F(k-i+2)-2(i+1)(k-i+1)F(i+1)F(k-i+1)\right] \quad (35)$$
$$+\left[\frac{1}{\phi_1}K_p+\frac{\phi_4}{\phi_2}M\right]\left[\delta(k)-(k+1)F(k+1)\right]+2\delta(k)+G_rG(k)+G_cH(k)=0,$$
$$\left[\frac{k_{nf}/k_f}{\phi_3}+\frac{R/k_f}{\phi_3}\right](k+1)(k+2)G(k+2)$$
$$+P_r\sum_{i=0}^{k}\left[(k-i+1)F(i)G(k-i+1)-(k-i+1)F(k-i+1)G(i)\right] \quad (36)$$
$$+P_r\left[\frac{(k+1)(k+2)F(k+2)}{\phi_3}\frac{E_c}{(1-\phi)^{2.5}}+\frac{Q}{\phi_3}G(k)\right]=0,$$
$$(k+1)(k+2)H(k+2)-S_cR_cH(k)$$
$$+S_c\sum_{i=0}^{k}\left[(k-i+1)F(i)H(k-i+1)-(k-i+1)F(k-i+1)H(i)\right]=0. \quad (37)$$

Substituting (32)-(34) in the above iterative formulae, F(k), G(k) and H(k)can be determined. Applying inverse transformation, the solutions of (14)-(16)subjected to the conditions (17) and (18) are obtained as

$$f(\eta)=\sum_{k=0}^{\infty}F(k)\eta^k\approx\sum_{k=0}^{n_1}F(k)\eta^k \quad (38)$$
$$\theta(\eta)=\sum_{k=0}^{\infty}G(k)\eta^k\approx\sum_{k=0}^{n_2}G(k)\eta^k \quad (39)$$
$$\gamma(\eta)=\sum_{k=0}^{\infty}H(k)\eta^k\approx\sum_{k=0}^{n_3}H(k)\eta^k \quad (40)$$

4.1 Padé approximant

Let $f(x)=\sum_{i=0}^{\infty}a_ix^i$ be the power series of f(x).

(41)

The Padé approximant isexpressedas

$$[L,M]=\frac{R_L(x)}{S_M(x)}, \quad (42)$$

where $R_L(x)$ and $S_M(x)$ are at most L[th] and M[th] degree polynomials respectively as

$$f(x)=a_0+a_1x+a_2x^2+a_3x^3+a_4x^4+....., \quad (43)$$
$$R_L(x)=r_0+r_1x+r_2x^2+r_3x^3+r_4x^4+.....+r_Lx^L, \quad (44)$$
$$S_M(x)=s_0+s_1x+s_2x^2+s_3x^3+s_4x^4+.....+s_Mx^M, \quad (45)$$

From equation (42), we have L+1 numerator coefficients and M+1 denominator coefficients. [L; M] can be left unchanged by multiplying a constant with the numerator and denominator. The normalization condition is taken as

$$S_M(0)=1 \quad (46)$$

Now L+M +1 unknown coefficient are there in total. It describes that the [L;M] fits the power series equation(41) with the orders $1, x, x^2, x^3, ..., x^{L+M}$ and is uniquely determined.

$$\text{So, } \sum_{i=0}^{\infty} a_i x^i = \frac{r_{0+} r_1 x + r_2 x^2 + r_3 x^3 + ... + r_L x^L}{s_{0+} s_1 x + s_2 x^2 + s_3 x^3 + ... + s_M x^L} + O(x^{L+M+1}). \tag{47}$$

From (47), we get

$$\begin{aligned}&(a_0 + a_1 x + a_2 x^2 + a_3 x^3 + a_4 x^4 + ...)(s_0 + s_1 x + s_2 x^2 + s_3 x^3 + ... + s_M x^M) \\ &= r_0 + r_1 x + r_2 x^2 + r_3 x^3 + ... + r_L x^L + O(x^{L+M+1})\end{aligned} \tag{48}$$

Equation (48) gives

$$\begin{cases} a_0 = r_0, \\ a_1 + a_0 s_1 = r_1 \\ a_2 + a_1 s_1 + a_0 s_2 = r_2 \\ . \\ . \\ . \\ a_L + a_{L-1} s_1 + ... + a_0 s_L = r_L, \end{cases} \tag{49}$$

and

$$\begin{cases} a_{L+1} + a_L s_1 + ... + a_{L-M+1} s_M = 0, \\ a_{L+2} + a_{L+1} s_1 + ... + a_{L-M+2} s_M = 0, \\ \vdots \\ a_{L+M} + a_{L+M-1} s_1 + ... + a_L s_M = 0. \end{cases} \tag{50}$$

where $a_n = 0$ for n < 0 and $s_j = 0$ for j > M. Equations(49) and (50) can be solved directly if these are nonsingular.

$$[L,M] = \frac{\begin{vmatrix} a_{L-M+2} & a_{L-M+2} & \cdots & a_{L+1} \\ \vdots & \vdots & \ddots & \vdots \\ a_L & a_{L+1} & \cdots & a_{L+M} \\ \sum_{j=M}^{L} a_{j-M} x^j & \sum_{j=M-1}^{L} a_{j-M+1} x^j & \cdots & \sum_{j=0}^{L} a_j x^j \end{vmatrix}}{\begin{vmatrix} a_{L-M+1} & a_{L-M+2} & \cdots & a_{L+1} \\ \vdots & \vdots & \ddots & \vdots \\ a_L & a_{L+1} & \cdots & a_{L+M} \\ x^M & x^{M-1} & \cdots & 1 \end{vmatrix}} \tag{51}$$

The sum is replaced by zero if the lower index on a sum exceeds the upper, Other forms are

$$\begin{aligned}[L,M] &= \sum_{j=0}^{L-M} a_j x^j + x^{L-M+1} w_{L/M}^T W_{L/M}^{-1} w_{L/M} \\ &= \sum_{j=0}^{L+n} a_j x^j + x^{L+n+1} w_{(L+1)/M}^T W_{L/M}^{-1} w_{(L+n)/M},\end{aligned} \tag{52}$$

for

$$W_{L,M} = \begin{bmatrix} a_{L-M+1} - x a_{L-M+2} & \cdots & a_L - x a_{L+1} \\ \vdots & \ddots & \vdots \\ a_L - x a_{L+1} & \cdots & a_{L+M+1} - x a_{L+M} \end{bmatrix} \tag{53}$$

$$w_{L,M} = \begin{bmatrix} a_{L-M+1} \\ a_{L-M+2} \\ \vdots \\ a_L \end{bmatrix} \tag{54}$$

[L; M] approximants construction comprises algebraic operations only. The objective of the technique is to get the best approximant. It needs the utilization of a criterion depending on the shape of the solution. The diagonal approximant is the most accurate approximant; so,the diagonal approximants is constructed. After getting series solutions (38)-(40), the Padé approximation is utilized. In Eq. (42), the value of i is taken as 50. The accuracy of the solution increases with increase in order of Padé approximation.

4.2 Numerical solution

The fourth order Runge-Kutta method with shooting technique is used to solve equations (14) to (16) with boundary conditions (17) and (18).

Substituting $f = y_1, f' = y_2, f'' = y_3, \theta = y_4, \theta' = y_5, \gamma = y_6, \gamma' = y_7$ in equations (14) to (18), we get the simplified equations and boundary conditions as follows

$$y_3' = \phi_1\left[-y_1 y_3 - 2(1-y_2^{\,2}) - \left(\frac{P}{\phi_1} + \frac{\phi_4}{\phi_2}M\right)(1-y_2) - G_r y_4 - G_c y_6\right],$$

$$y_5' = \frac{\left[-P_r(y_1 y_5 - y_2 y_4) - \dfrac{E_c P_r y_3}{\phi_3(1-\phi)^{2.5}} - \dfrac{P_r Q y_5}{\phi_3}\right]}{\left[\dfrac{k_{nf}}{\phi_3 k_f} + \dfrac{R}{\phi_3 k_f}\right]},$$

$$y_7' = -S_c(y_1 y_7 - y_2 y_6) - \lambda y_6,$$

$$y_1 = S, y_2 = 0, y_4 = 1, y_6 = 1 \text{ at } \eta = 0,$$
$$y_2 = 1, y_4 = 0, y_6 = 0 \text{ as } \eta \to \infty.$$

To apply the Runge-Kutta method along with shooting technique, MATLAB code with a step length of 0.001 and error bound 10^{-3} is implemented, guessing the values of y_3, y_5 and y_7.

5. Results

The present investigation embarks upon the interaction of buoyancy forces modifying the momentum transport and accounting for the thermal energy due to viscous dissipation and presence of volumetric heat source/sink; an extended contribution to heat equation in the present model. Further, adoption of two methods of solutions both numerical as well as approximate analytical DTM enriches the study ensuring the validity of the results pertaining to nanofluid enhancing the thermal energy transport phenomena.

The inclusion of space dependent oscillatory free stream (potential flow) induces oscillations in temperature and concentration on the bounding surface as well as value of chemical reaction. Further, consideration of suction/injection at the bounding surface is a suggestive measure for the growth of boundary layer and consequently flow reversal. The thermophysical properties of base fluid (water) and metals (Cu and Ag) and metallic oxide (Al_2O_3) which constitute the nanoparticles, are enumerated in Table.1. The computation of volumetric entropy generation accounting for the thermal energy due to viscous dissipation, joule heating, Darcy dissipation along with thermal and solutal gradients contributing to diffusion processes enrich the present analysis. Figures 2-5 shows the effects of Q, G_r, G_c and Br on velocity distribution. The impacts of Br and Q are depicted in Figures 6 and 7. Figures 8-11 represent the entropy generation profiles against the parameters Q, G_r, G_c and Br respectively. In Figure 12, a comparison is made between the present results with the earlier results (Zhang et al.,

2014). Figure 13 presents the effect of different water based nanofluids of metals (Cu & Ag) and oxide (Al_2O_3) on the velocity field. The skin friction coefficient, which quantifies the shearing stress on the plate's surface, varies over the Brinkman number space for the nanofluids Al_2O_3-water and Cu-water in Fig. 14. Figure 15 illustrates the variation of local Nusselt number against Brinkman number for different nanofluid. A comparison between DTM-Pade approximation solution and numerical solution is made in Figure 16. The effects of solid volume fraction ϕ on velocity and temperature are depicted in Figures 17 & 18.

Except where otherwise noted, the values of the parameters are taken to be S=1, ϕ =0.1, ϕ_1 =0.7002, ϕ_2 =0.9112, ϕ_3 =1.0212, ϕ_4 =0.9, M =1, K_p=0.5, Pr=0.7, G_r = 1, G_c = 1, Ec=0.01, Q=0.5, R = 1, Sc = 1, Br=0.5, Ha=0.5 .

6. Discussion

The following discussion is pertaining to Cu-water working nanofluid with fixed values of parameters as mentioned above except Fig.3.

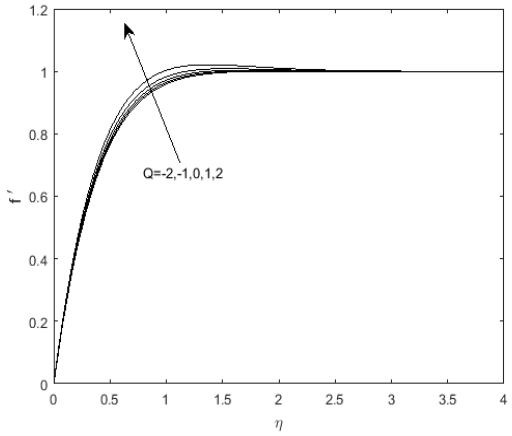

Figure 2: Velocity profiles for Q

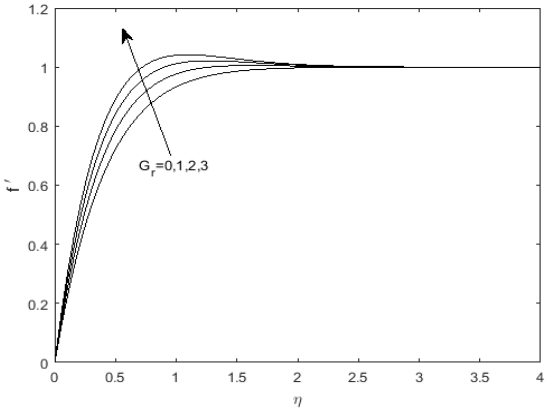

Figure 3: Velocity profiles for G_r

Fig. 2 shows that sharp rise in velocity in the neighborhood layers of the bounding surface to attain the prescribed free stream velocity with a slight increase due to increase in the strength of heat power.

Figures 3, 4 and 5 depict the slight increase in velocity with increasing values of thermal as well as solutal boundary parameters and Brinkman number (P_r.E_c), which indicates how important viscous heating is in relation to the heat flow caused by the impressed temperature difference between the free stream and bounding surface ($T_w - T_\infty$) (Bansal (1997)). It's noteworthy to observe that, in comparison to G_c and B_r, the effect of the thermal boundary is not as important.

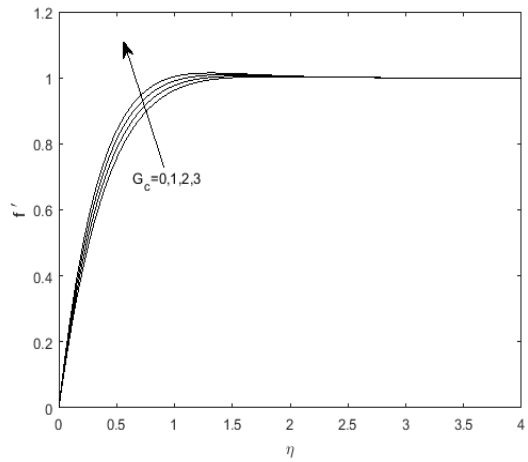

Figure 4: Velocity profiles for G_c

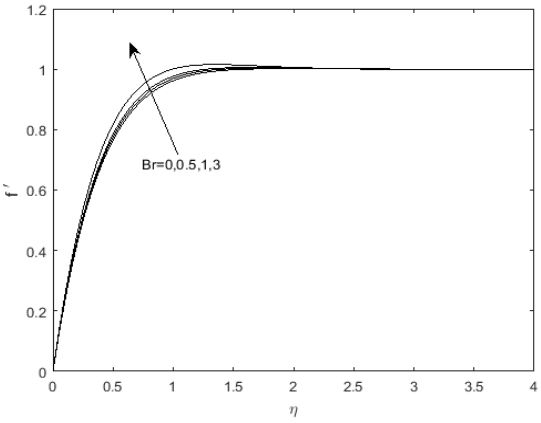

Figure 5: Velocity profiles for Br

Figure 6 depicts the effect of Brinkman number B_r ($Br = E_c P_r$). It is interesting to observe that there is a hike in temperature near the wall for higher value of B_r ($Br = 3$) but for others the variation is smooth, i.e., quantitatively it can be said that temperature increases commensurately by approx. 40% with increase in Br. This indicates that the viscous heating is dominant in the neighborhood of the plate for higher value of Br and for small values; the distribution is smooth across the flow field.

Fig.7 shows the similar variation for higher values of heat source parameter. Quantitatively we can say that temperature increases commensurately by approx. 40% with increase in Q.

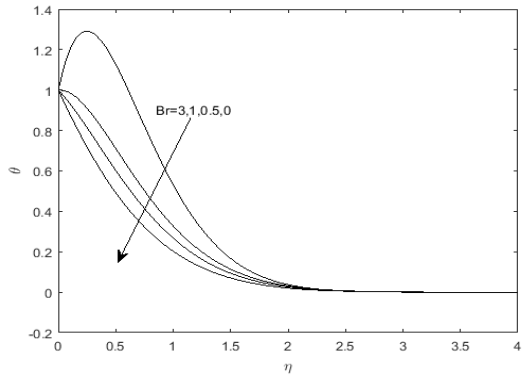

Figure 6: Temperature profiles for Br

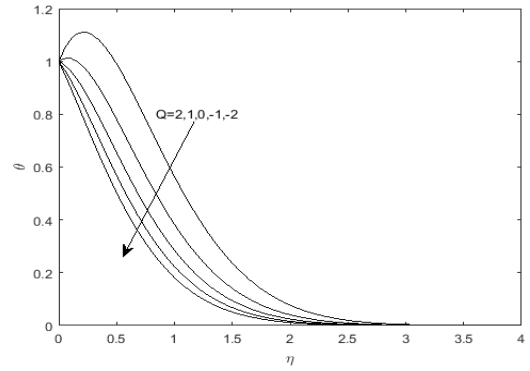

Figure 7: Temperature profiles for Q

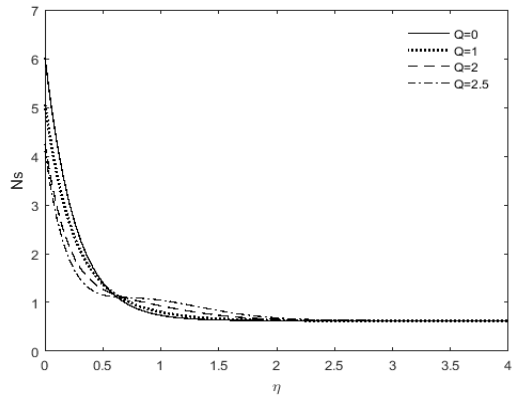

Figure 8: Entropy generation number for Q

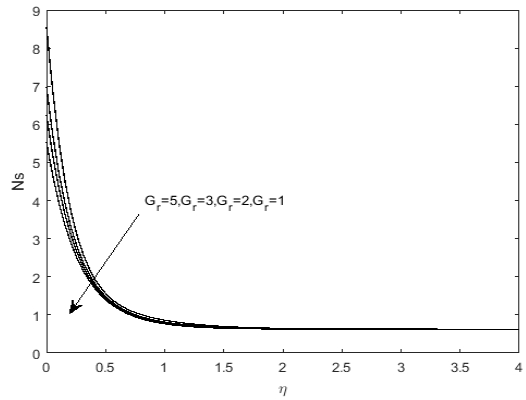

Figure 9: Entropy generation number for G_r

Figure 8 shows the entropy variation for different values of heat source parameter. It is interesting to note that the entropy generation decreases with an increase in the strength of heat source in the neighborhood layers upto $\eta \approx 0.5$, there after it increases. This shows that entropy generation becomes independent of embodied heat power at a certain layer of flow field. This result is a bearing in the arena of various heat transport phenomena.

Fig. 9 and 10 show the effect of Gr and Gc, the buoyancy forces on entropy generation. The entropy generation increases with an increase in the values of Gr and Gc within a few layers in the neighborhood of the plate surface and there after asymptotic variation is marked.

Figure 11 provides a striking outcome in respect of entropy generation for various values of Brinkman number. The common feature is increase in entropy generation for higher values of Br in a streamline manner within asymptotic pattern. This result is important in its own revelation and application basis. Figure 12 provides the validity of the solution methods applied and results obtained in the present analysis (with Zhang et al. (2014)).

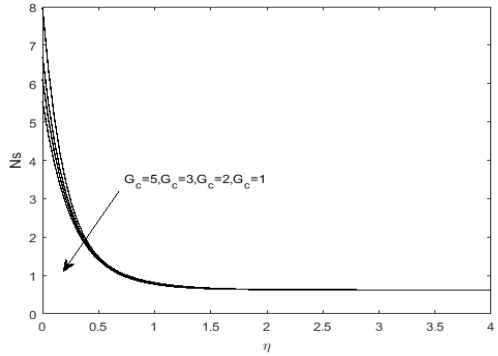

Figure 10: Entropy generation number for G_c

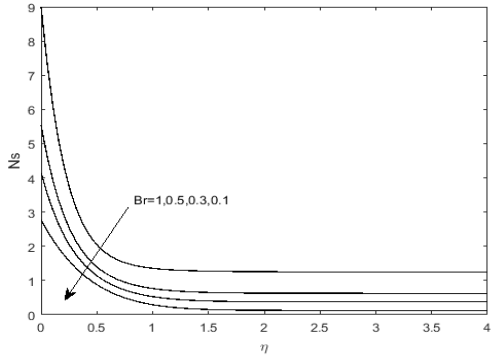

Figure 11: Entropy generation number for Br

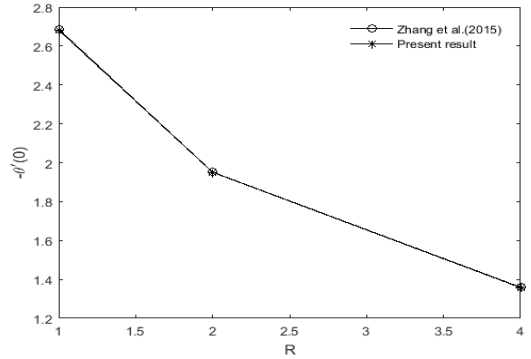

Figure 12: Comparison of $-\theta'(0)$ with Zhang et al.[34] for different values of R when $\phi = 0.1, \Pr = 6.2$

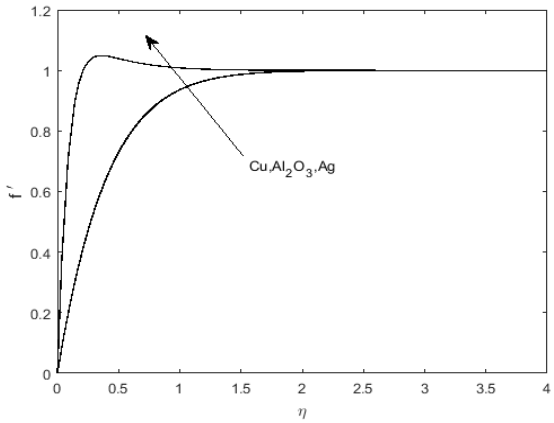

Figure 13: Velocity profiles for different types of nanofluids

Fig. 13 depicts the efficiency of Ag-water nanofluid over other Cu-water and Al_2O_3-water nanofluids. The momentum transport is accelerated to enhance the velocity across the flow domain, but Cu-water and Al_2O_3-water do not show any significant difference. The important outcomes are: metallic oxide is as efficient as metal. Secondly, silver nanoparticles are superior to Cu in enhancing momentum diffusion across flow field. It is noteworthy to note in Figure 14 that skin friction increases continuously with larger values of the Brinkman number and that metallic oxide offers a higher rate of skin friction than the metal (Cu). Thus, it can be deduced that skin friction causes viscous heating that is proportional to the Brinkman number. The Nusselt number, or heat transfer coefficient, in Brinkman-space, which quantifies the amount of heat transmitted from the bounding surface to fluid in the Brinkman-space, varies as shown in Fig. 15. It can be shown that the heat transfer coefficient is modest and stays constant with respect to Ag, but it continually declines when the Brinkman number rises. This

result is quite helpful if the design specification calls for consistent heat transfer from the solid surface to fluid regardless of viscous heat generation, in which case Ag-water nanofluid is advised.

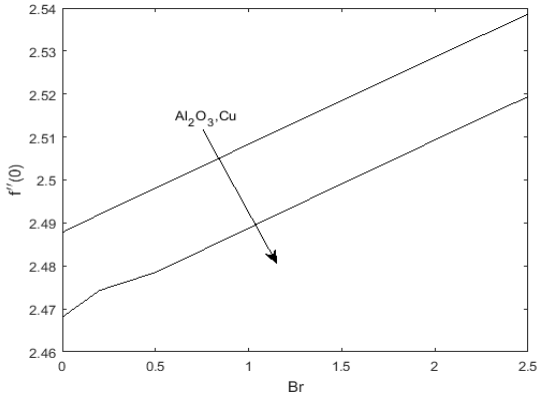

Figure 14: Local skinfriction for Cu-water and Al_2O_3-water nanofluids

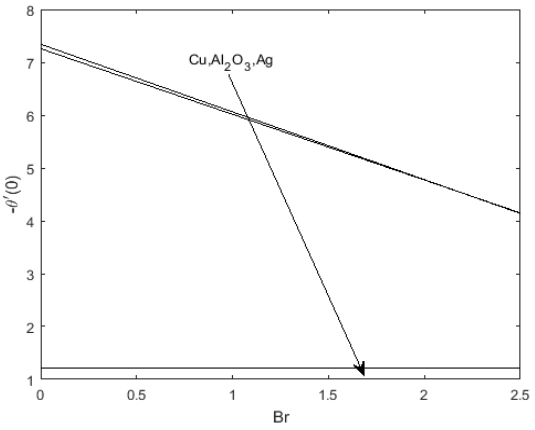

Figure 15: Local Nussselt number for different nanofluids

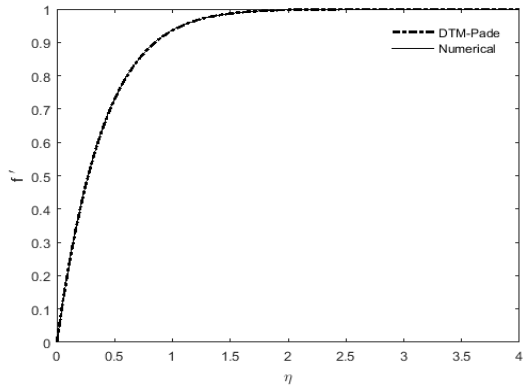

Figure 16: Comparison between DTM-Padé and Numerical method

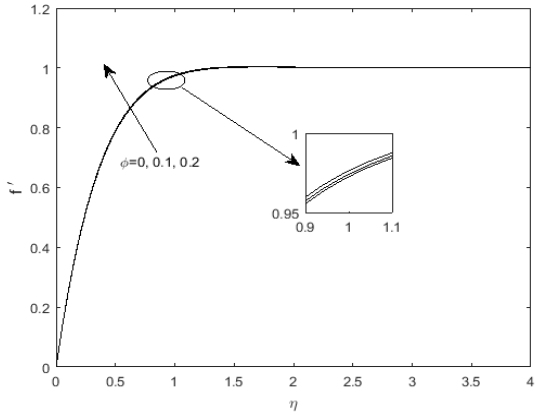

Figure 17: Velocity profiles for ϕ

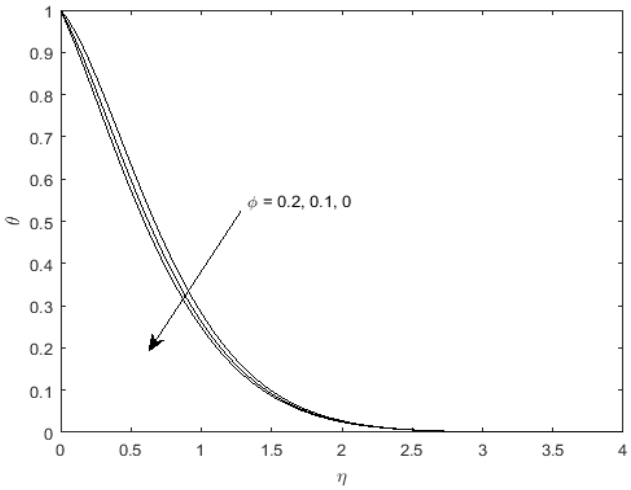

Figure 18. Temperature profiles for ϕ

Fig.16 shows the compatibility of results obtained from DTM- Padé approximation and numerical method (shooting technique with Runge-Kutta 4th order method).

Figures 17 and 18 show the impact of the solid volume fraction of nanoparticles on the distributions of velocity and temperature for Cu-water nanofluid. With an increase in the solid volume fraction, it is discovered that both velocity and temperature rise. These results are in good agreement with the results of Zhang et al. (2014).

7. Conclusion

By taking into account the heat source and chemical reaction, a flat plate embedded in a porous medium is used to study the dissipative MHD nanofluid flow with uniform suction/blowing. The governing partial differential equations are converted into a set of non-linear ordinary differential equations using similarity transformation. These non-linear ordinary differential equations are then solved numerically using the shooting technique and the Runge-Kutta 4^{th} order method, as well as by the differential transform method with Padé approximantion. Graphs are used to discuss the effects of some important parameters. Below are a few key conclusions.

- Viscous heating is dominant in the neighbourhood of the plate for higher value of Br and for small values the distribution is smooth across the flow field.
- Velocity is slightly increased with increasing values of thermal as well as solutal boundary parameters and Brinkman number.
- Entropy generation becomes independent of embodied heat power at a certain layer of flow field. This result is a bearing in the arena of various heat transport phenomena.
- Entropy generation is decreased for higher values of Br in a streamline manner within asymptotic pattern. This shows there is a base value or residue left over energy in the process of entropy generation.
- Silver nanoparticles are superior to Cu in enhancing momentum diffusion across flow field.
- The skin friction commensurate with Brinkman number i.e generation of viscous heating.
- If the design requirement needs a constant heat transfer from the solid surface to fluid irrespective of viscous heat generation then Ag-water nanofluid is recommended.
- Temperature increases commensurately by approx. 40% with increase in both Br and Q within the range $0<Br<1$, $-2<Q<1$.
- Entropy generation increases commensurately by approx. 95% with increase in Br within the range $0.1<Br<0.5$.

References

Ali, A., Vafai, K. and Khaled, A.-R.A. (2003): Comparative study between parallel and counter flow configurations between air and falling film desiccant in the presence of nanoparticle suspensions, International Journal of Energy Research 27, 725-745. https://doi.org/10.1002/er.908

Ali , B. , Hussain , S. , Nie , Y. , Hussein, A.K. and Habib , D. (2021): Finite element investigation of Dufour and Soret impacts on MHD rotating flow of Oldroyd-B nanofluid over a stretching sheet with double diffusion Cattaneo Christov heat flux model , Powder Technology , 377 , 439-452. https://doi.org/10.1016/j.powtec.2020.09.008

Ali, L., Omar, Z., Khan I., Seikh, A.H., Sherif E.M. and Nisar K.S. (2019): Stability analysis and multiple solution of Cu-Al2O3/H2O nanofluid contains hybrid nanomaterials over a shrinking surface in the presence of viscous dissipation. J Mater Res Technol 9(1):421- 432. https://doi.org/10.1016/j.jmrt.2019.10.071

Aravind, S. S. J., Baskar, P., Baby, T. T., Sabareesh, R. K., Das, S. and Ramaprabhu, S. (2011): Investigation of structural stability, dispersion, viscosity, and conductive heat transfer properties of functionalized carbon nanotube based nanofluids, The Journal of Physical Chemistry C, 115, 16737-16744. https://doi.org/10.1021/jp201672p

Bachok, N., Ishak, A. and Pop, I. (2013): Boundary layer stagnation-point flow toward a stretching/ shrinking sheet in a nanofluid, J. Heat Transfer, 135, 054501. https://doi.org/10.1115/1.4023303

Bagh , A. , Khan , S. , Hussein , A.K , Thumma , T. and Hussain , S (2022): Hybrid nanofluids : significance of gravity modulation , heat source/sink , and magnetohydrodynamic on dynamics of micropolar fluid over an inclined surface via finite element simulation , Applied Mathematics and Computation , 419, Article No.126878. https://doi.org/10.1016/j.amc.2021.126878

Bansal, J.L.: (1997), Viscous Fluid Dynamics, Oxford, pp.61.

Bejan, A., (1982): Second law analysis in heat transfer and thermal design, Advances in Heat Transfer, 15 1-58.

Bejan, A.(1996): Entropy Generation Minimization, CRC Press, Boca Raton, New York.
Bi, S., Shi, L. and Zhang, L. (2008): Application of nanoparticles in domestic refrigerators, Applied Thermal Engineering, 28, 1834-1843. https://doi.org/10.1016/j.applthermaleng.2007.11.018
Biswal, M.M., Swain, B.K., Das, M. and Dash, G.C. (2022): Heat and mass transfer in MHD stagnation point flow toward an inclined stretching sheet embedded in a porous medium, Heat Transfer, 2022, https://doi.org/10.1002/htj.22525.
Biswal , U. , Chakraverty , S. , Ojha , B. and Hussein , A.K. (2022): Numerical investigation on nanofluid flow between two inclined stretchable walls by optimal homotopy analysis method, Journal of Computational Science , 63 , Article No. 101759. https://doi.org/10.1016/j.jocs.2022.101759
Choi, S. U. S. (2009): Nanofluids: From vision to reality through research, Journal of Heat Transfer, 131, 33106-33109. https://doi.org/10.1115/1.3056479
Haque, M.E., Bakar, R.A., Kadirgama, K., Noor, M.M. and Shakaib, M. (2016): Performance of a domestic refrigerator using nanoparticles-based polyolester oil lubricant. Journal of Mechanical Engineering and Sciences, 10, 1778-1791. http://dx.doi.org/10.15282/jmes.10.1.2016.3.0171
Hussain, S. (2017): Finite element solution for MHD flow of nanofluids with heat and mass transfer through a porous media with thermal radiation, viscous dissipation and chemical reaction effects, Advances in Applied Mathematics and Mechanics, 9(4), 904-923. https://doi.org/10.4208/aamm.2014.m793
Ijam, A., Saidur, R., Ganesan, P. and Golsheikh, A. M. (2015): Stability, thermo-physical properties, and electrical conductivity of graphene oxide-deionized water/ethylene glycol based nanofluid. International Journal of Heat and Mass Transfer, 87, 92-103. https://doi.org/10.1016/j.ijheatmasstransfer.2015.02.060
Jusoh, R., Nazar, R. and Pop, I. (2019): Magnetohydrodynamic boundary layer flow and heat transfer of nanofluids past a bidirectional exponential permeable stretching/shrinking sheet with viscous dissipation effect. Journal of Heat Transfer 141(1), 012406. https://doi.org/10.1115/1.4041800
Kameswaran, P.K., Narayana, M., Sibanda, P. and Murthy, PVSN (2012): Hydromagnetic nanofluid flow due to a stretching or shrinking sheet with viscous dissipation and chemical reaction effects. International Journal of Heat and Mass Transfer, 55, 7587-7595. https://doi.org/10.1016/j.ijheatmasstransfer.2012.07.065
Kameswaran, P.K., Sibanda P., RamReddy C., Murthy P.V.S.N. (2013): Dual solutions of stagnation-point flow of a nanofluid over a stretching surface, Boundary Value Problems, 2013, 188. https://doi.org/10.1186/1687-2770-2013-188
Khanafer, K. and Vafai, K. (2011): A critical synthesis of thermophysical characteristics of nanofluids, International Journal of Heat and Mass Transfer, 54, 4410-4428. https://doi.org/10.1016/j.ijheatmasstransfer.2011.04.048
Ladjevardi, S. M., Asnaghi, A., Izadkhast, P. S. and Kashani, A. H. (2013): Applicability of graphitenanofluids in direct solar energy absorption, Solar Energy, 94, 327-334. https://doi.org/10.1016/j.solener.2013.05.012
Mabood, F., Khan, W.A. and Ismail, A.I.M. (2015): MHD boundary layer flow and heat transfer of nanofluids over a nonlinear stretching sheet: a numerical study, Journal of Magnetism and Magnetic Materials, 374, 569-576. https://doi.org/10.1016/j.jmmm.2014.09.013
Mahatha, B.K., Nandkeolyar, R. , Nagaraju, G. and Das, M. (2015): MHD stagnation point flow of a nanofluid with velocity slip, nonlinear radiation and Newtonian heating, Procedia Eng. 127, 1010-1017. https://doi.org/10.1016/j.proeng.2015.11.450
Mansur S., Ishak A. and Pop I. (2015): The magnetohydrodynamic stagnation point flow of a nanofluid over a stretching/ shrinking sheet with suction, PLoS ONE, 10, 1-14. https://doi.org/10.1371/journal.pone.0117733
Mohamed M.K.A., Noar N.A.Z., Salleh M.Z., Ishak A. (2015): Stagnation point flow past a stretching sheet in a nanofluid with slip condition, AIP Conferene Proceedings 1643, 635-641. https://doi.org/10.1063/1.4907505
Mustafa, M., Hayat, T., Pop, I., Asghar, S. and Obaidat, S. (2011): Stagnation-point flow of a nanofluid towards a stretching sheet, International Journal of Heat and Mass Transfer, 54, 5588-5594. https://doi.org/10.1016/j.ijheatmasstransfer.2011.07.021
Parida, B.C., Swain, B.K. and Senapati, N. (2021): Mass transfer effect on viscous dissipative MHD flow of nanofluid over a stretching sheet embedded in a porous medium. Journal of Naval Architecture and Marine Engineering, 18, 73-82. https://doi.org/10.3329/jname.v18i1.53380
Sadeghinezhad, E., Mehrali, M., Saidur, R., Mehrali, M., Latibari, S. T., Akhiani, A. R., and Metselaar, H. S. C. (2016): A comprehensive review on graphene nanofluids: Recent research, development and applications, Energy Conversion and Management, 111, 466-487. https://doi.org/10.1016/j.enconman.2016.01.004
Shafahi, M., Bianco, V., Vafai, K. and Manca, O. (2010): Thermal performance of flat-shaped heat pipes using nanofluids. International Journal of Heat and Mass Transfer, 53, 1438-1445. https://doi.org/10.1016/j.ijheatmasstransfer.2009.12.007

Shahi, M., Mahmoudi, A.H. and Raouf, A.H., (2011): Entropy generation due to natural convection cooling of a nanofluid, International Communications in Heat and Mass Transfer, 38 (7), 972-983. https://doi.org/10.1016/j.icheatmasstransfer.2011.04.008

Sheikholeslami M., Abelman S. and Domiri G. D. (2014): Numerical simulation of MHD nanofluid flow and heat transfer considering viscous dissipation. International Journal of Heat and Mass Transfer, 79, 212-222, https://doi.org/10.1016/j.ijheatmasstransfer.2014.08.004

Sohel, M.R., Saidur, R., Hassan, N.H., Elias, M.M., Khaleduzzaman, S.S. and MahbubulI, M. (2013): Analysis of entropy generation using nanofluid flow through the circular microchannel and minichannel heat sink, Int. Commun. Heat Mass Transfer, 46, 85-91. https://doi.org/ 10.1016/j.icheatmasstransfer.2013.05.011.

Swain, B.K. (2021): Effect of Second Order Chemical Reaction on MHD Free Convective Radiating Flow over an Impulsively Started Vertical Plate, Journal of Nonlinear Modeling and Analysis, 3, 167-178. https://doi.org/10.12150/jnma.2021.167

Swain, B.K., Biswal, M.M. and Dash, G.C. (2021): Effect of the second-order slip and heat source on dissipative MHD flow of blood through a permeable capillary in stretching motion, International Journal of Ambient Energy, https://doi.org/10.1080/01430750.2021.1979649.

Swain, B.K., Parida, B.C., Kar, S. and Senapati N. (2020): Viscous dissipation and Joule heating effect on MHD flow and heat transfer past a stretching sheet embedded in a porous medium. Heliyon, 6, 1-8. https://doi.org/10.1016/j.heliyon.2020.e05338

Syuhada, N., Ari, N. and Nazar, R. (2019): Stability analysis of unsteady MHD stagnation point flow and heat transfer over a shrinking sheet in the presence of viscous dissipation, Chinese Journal of Physics, 57, 116-126. https://doi.org/10.1016/j.cjph.2018.12.005

Zhang, C., Zheng, L., Zhang, X. and Chen, G., (2014): MHD flow and radiation heat transfer of nanofluids in porous media with variable surface heat flux and chemical reaction, Applied Mathematical Modelling, http://dx.doi.org/10.1016/j.apm.2014.05.023.